

Controlling and leveraging small-scale information in tomographic galaxy-galaxy lensing

Niall MacCrann^{1,2*}, Jonathan Blazek³, Bhuvnesh Jain⁴ and Elisabeth Krause⁵

¹ Center for Cosmology and Astro-Particle Physics, The Ohio State University, Columbus, OH 43210, USA

² Department of Physics, The Ohio State University, Columbus, OH 43210, USA

³ Institute of Physics, Laboratory of Astrophysics, École Polytechnique Fédérale de Lausanne (EPFL), Observatoire de Sauverny, 1290 Versoix, Switzerland

⁴ Department of Physics and Astronomy, University of Pennsylvania, Philadelphia, PA 19104, USA

⁵ Department of Astronomy/Steward Observatory, 933 North Cherry Avenue, Tucson, AZ 85721-0065, USA

Accepted XXX. Received YYY; in original form ZZZ

ABSTRACT

The tangential shear signal receives contributions from physical scales in the galaxy-matter correlation function well below the transverse scale at which it is measured. Since small scales are difficult to model, this non-locality has generally required stringent scale cuts or new statistics for cosmological analyses. Using the fact that uncertainty in these contributions corresponds to an uncertainty in the enclosed projected mass around the lens, we provide an analytic marginalization scheme to account for this. Our approach enables the inclusion of measurements on smaller scales without requiring numerical sampling over extra free parameters. We extend the analytic marginalization formalism to retain cosmographic (“shear-ratio”) information from small-scale measurements that would otherwise be removed due to modeling uncertainties, again without requiring the addition of extra sampling parameters. We test the methodology using simulated likelihood analysis of a DES Year 5-like galaxy-galaxy lensing and galaxy clustering datavector. We demonstrate that we can remove parameter biases due to the presence of an un-modeled 1-halo contamination of the galaxy-galaxy lensing signal, and use the shear-ratio information on small scales to improve cosmological parameter constraints.

Key words: gravitational lensing; weak – cosmological parameters

1 INTRODUCTION

The observed shapes of distant galaxies are distorted due to variations in the gravitational potential experienced by emitted light on its path to the observer, an effect known as gravitational lensing. In the weak lensing regime, a small change in the observed ellipticity of such a *source* galaxy is generated, known as a shear. Coherent structure in the intervening density field generates coherent patterns in the observed shear field. For example, a net tangential alignment or *tangential shear* of source galaxies is produced around overdense regions in the intervening density field.

Since galaxies also trace overdense regions, we can measure the average tangential shear of source galaxies around these tracers, also known as *lens* galaxies, to probe the relationship between lens galaxy and matter densities. This sort of measurement is known as *galaxy-galaxy lensing*, and since

early detections by Tyson et al. (1984) and Brainerd et al. (1996), it has been measured at increasing signal-to-noise (e.g. Choi et al. 2012; Cacciato et al. 2013; Mandelbaum et al. 2013; Velander et al. 2014; Clampitt et al. 2017; Prat et al. 2018b), and precision measurements from state-of-the-art photometric imaging surveys have been used for cosmological parameter estimation (DES Collaboration et al. 2017; van Uitert et al. 2018; Joudaki et al. 2018; Singh et al. 2018).

The galaxy-galaxy lensing signal depends on the total matter distribution around the lens galaxies, or the galaxy-matter cross-correlation function $\xi_{\text{gm}}(r)$. In the halo-model picture (Seljak 2000; Peacock & Smith 2000), on small scales the measurement is most sensitive to the properties of the halos populated by the lens galaxies, for example the mean halo mass. Hence galaxy-galaxy lensing has been used to characterize the relation between halo mass and baryonic content of galaxies (e.g. Leauthaud et al. 2012; Viola et al. 2015; van Uitert et al. 2016). On larger scales, galaxy-galaxy lensing has been combined with galaxy clustering to simulta-

* E-mail: maccrann.2@osu.edu

neously constrain the galaxy bias, and cosmological parameters, in particular the matter density and matter clustering amplitude at low redshift. Especially when combined with external constraints from e.g. the cosmic microwave background, this combination can also provide competitive constraints on the dark energy equation of state (Weinberg et al. 2013). These constraints will only improve with upcoming stage IV surveys such as the Large Synoptic Survey Telescope¹ (LSST), Euclid² and the Wide-Field Infrared Survey Telescope³ (WFIRST), which will dramatically increase the volume of high quality weak-lensing data available.

There are typically significant observational and theoretical challenges in performing a galaxy-galaxy lensing analysis (Mandelbaum 2018). In the former category, the shear must be estimated with high accuracy from images of faint source galaxies that are typically noisy and blurred by a point spread function, an ongoing challenge in the weak lensing community (e.g. Bridle et al. 2009; Kitching et al. 2012; Mandelbaum et al. 2014). Furthermore, interpreting the signal requires redshift information for both lens and source galaxies, which generally requires estimating photometric redshifts from noisy flux estimates in a small number (typically around 5) of optical or near-infrared bands (e.g. Hildebrandt et al. 2017; Hoyle et al. 2018; Tanaka et al. 2018).

There are also significant theoretical challenges when attempting to model the galaxy-galaxy lensing signal, which generally becomes more difficult at smaller scales. In order to predict the signal, an accurate prediction for the galaxy-matter correlation function $\xi_{\text{gm}}(r)$ is required for some range of physical scales r . On sufficiently large scales we expect linear bias to hold (e.g. Fry & Gaztanaga 1993; Kaiser 1984), such that $\xi_{\text{gm}}(r) = b\xi_{\text{mm}}(r)$, where b is the linear galaxy bias, an unknown constant that can be marginalized over and $\xi_{\text{mm}}(r)$ is the matter correlation function. A higher-order perturbative modelling approach may be successful in predicting $\xi_{\text{gm}}(r)$ at smaller, mildly nonlinear scales (see Desjacques et al. 2018 for a recent review). A perturbative approach will likely fail on scales approaching the 1-halo regime, but here a model which assumes some halo occupation distribution (Peacock & Smith 2000; Seljak 2000; Berlind & Weinberg 2002; Wechsler & Tinker 2018) combined with an accurate prediction for the clustering of dark matter halos may be successful (e.g. Cacciato et al. 2013; Nishimichi et al. 2018; Wibking et al. 2019). Even this approach will break down on galactic scales where galactic astrophysics will affect the matter distribution in and around the lens galaxy.

The important point is that whatever modeling approach is taken, it is crucial to ensure that the measurement is only sensitive to scales in $\xi_{\text{gm}}(r)$ where that modelling approach is sufficiently accurate. In Section 2.1 we describe how the galaxy-galaxy signal receives a non-local contribution that depends on scales in $\xi_{\text{gm}}(r)$ that are much smaller than the separation at which the measurement is made (i.e. the impact parameter in the lens plane). It was this potential non-local contribution that motivated the use of a larger

minimum scale for galaxy-galaxy lensing than for galaxy clustering in the combined clustering, galaxy-galaxy lensing and cosmic shear analysis of Dark Energy Survey (DES) Year 1 data in Krause et al. (2017); DES Collaboration et al. (2017). We demonstrate how this non-local contribution can be accounted for in parameter estimation, and use analytic marginalization (Bridle et al. 2002) to avoid adding extra sampling parameters.

When galaxy-galaxy lensing of a given lens sample is measured from multiple sources redshifts, some limited information can be extracted even in the absence of a model for the galaxy-matter correlation function. This is often referred to as *shear-ratio* information; since the ratio of the signals measured from two different source redshifts depends only on the Universe’s geometry (Jain & Taylor 2003; Hu & Jain 2004; Bernstein & Jain 2004). In Section 3 we extend the aforementioned analytic marginalization formalism to allow the retention of shear-ratio information from small-scale galaxy-galaxy lensing measurements that would otherwise be excluded due to modelling uncertainties. Our use of analytic marginalization for both these problems makes our methods much more useful for cosmological parameter estimation from weak lensing surveys; without this the extra tens or hundreds of sampling parameters may lead to significant increases in convergence time for MCMC-based inference. We demonstrate the utility of our methodology by simulating cosmological parameter inference from a DES Year 5-like galaxy-galaxy lensing and galaxy clustering data vector in Section 4.

We conclude and discuss some potential limitations of the methodology in Section 5.

2 THE POINT-MASS CONTRIBUTION TO TANGENTIAL SHEAR

We start in Section 2.1 by describing how physical scales in ξ_{gm} contribute to the galaxy-galaxy lensing signal, and how the non-local contribution from small physical scales can be marginalized over. We draw in particular on Baldauf et al. (2010) (also see a recent treatment in Singh et al. 2018). We discuss the use of analytic marginalization in Section 2.2, and compare to the approach of Baldauf et al. (2010) in Section 2.3. We extend the formalism to a tomographic tangential shear measurement in Section 2.4.1, and demonstrate the effectiveness of our approach in recovering unbiased parameters in Section 2.5.

2.1 Theory

A lens galaxy sample at angular diameter distance D_l generates a mean tangential shear, $\gamma_t(\theta)$ (e.g. Hu & Jain 2004)

$$\gamma_t(\theta = R/D_l) = \frac{\Delta\Sigma(R)}{\Sigma_{\text{crit}}} \quad (1)$$

where

$$\Delta\Sigma(R) = \bar{\Sigma}(0, R) - \Sigma(R) \quad (2)$$

and $\Sigma(R)$ is the excess mean surface mass density at transverse physical separation R from the lens, given by the projection of the three-dimensional galaxy-matter correlation

¹ <http://www.lsst.org>

² <http://sci.esa.int/science-e/www/area/index.cfm?fareaid=102>

³ <http://wfirst.gsfc.nasa.gov>

function ξ_{gm} over line-of-sight distance Π :

$$\Sigma(R) = \bar{\rho}_m \int_{-\infty}^{\infty} d\Pi \left[1 + \xi_{\text{gm}} \left(\sqrt{R^2 + \Pi^2} \right) \right], \quad (3)$$

where $\bar{\rho}_m$ is the mean matter density. $\bar{\Sigma}(R_1, R_2)$ is the mean surface mass density averaged between R_1 and R_2

$$\bar{\Sigma}(R_1, R_2) = \frac{2}{R_2^2 - R_1^2} \int_{R_1}^{R_2} R' dR' \Sigma(R'). \quad (4)$$

Σ_{crit} is a geometrical factor that determines how the amplitude of the signal depends on lens and source redshift, and for a single source redshift plane at angular diameter distance D_s , is given by

$$\Sigma_{\text{crit}}^{-1} = \begin{cases} (1 + z_l) \frac{4\pi G}{c^2} \frac{D_l(D_s - D_l)}{D_s} & \text{if } D_s > D_l \\ 0 & \text{otherwise} \end{cases} \quad (5)$$

where z_l is the lens redshift.

The presence of $\bar{\Sigma}(0, R)$ in equation 2 makes clear the non-locality of $\Delta\Sigma(R)$ (and therefore $\gamma_t(\theta)$); this term depends on the distribution of mass around the lens on all scales up to R , or equivalently, on $\xi_{\text{gm}}(r)$ for all $0 < r < R$. As a consequence, $\Delta\Sigma(R)$ and $\gamma_t(\theta)$ can be sensitive to the mass distribution on one-halo scales, where a perturbative modeling approach will break down, even when measured at separations R that correspond to much larger physical scales in the lens plane. There is extensive discussion of this effect in Baldauf et al. (2010) who propose an estimator-based approach for dealing with this non-locality that we discuss in Section 2.3. We note here that a projected galaxy clustering measurement, $w_{\text{gg}}(R)$ does not suffer from this effect - here the minimum physical scale probed in the three-dimensional correlation function $\xi_{\text{gg}}(r)$ is the same as the transverse separation R .

If we assume we can model the galaxy-matter correlation function $\xi_{\text{gm}}(r)$ only down to some minimum scale r_{min} , we can account for the contribution from scales below r_{min} in the following way. For $R > r_{\text{min}}$ we can decompose $\bar{\Sigma}(0, R)$ into two terms

$$\bar{\Sigma}(0, R) = \frac{r_{\text{min}}^2 \bar{\Sigma}(0, r_{\text{min}})}{R^2} + \frac{(R^2 - r_{\text{min}}^2) \bar{\Sigma}(r_{\text{min}}, R)}{R^2}. \quad (6)$$

Only the first term in equation 6 is beyond our ability to model accurately (the second term requires only ξ_{gm} at $r > r_{\text{min}}$). This first term has $1/R^2$ scale dependence, so for $R > r_{\text{min}}$, any bias in our model due to inaccurate prediction of $\xi_{\text{gm}}(r < r_{\text{min}})$ has a simple $1/R^2$ scale dependence.

Hence, for $R > r_{\text{min}}$, we can model $\Delta\Sigma(R)$ as

$$\Delta\Sigma(R) = \Delta\Sigma^{\text{model}}(R) + B/R^2 \quad (7)$$

where $\Delta\Sigma^{\text{model}}(R)$ is the prediction based on a model for $\xi_{\text{gm}}(r)$ that is correct for scales $r > r_{\text{min}}$, but can be arbitrarily wrong for $r < r_{\text{min}}$, and B is some unknown constant that we can marginalize over.

Note that the first term in equation 6 is just the tangential shear contribution from the excess mass enclosed in a cylinder of radius r_{min} . For transverse scales R larger than r_{min} this has the same lensing signal as a point-mass located at $R = 0$, hence in the following we will refer to this contribution as the *point-mass* contribution. However, the constant B in equation 7 does not correspond exactly to this enclosed

mass if our model for $\xi_{\text{gm}}(r)$ makes a non-zero prediction for $\bar{\Sigma}(0, r_{\text{min}})$. In this case

$$B = \frac{\delta M}{\pi R^2 \Sigma_{\text{crit}}} \quad (8)$$

where δM is the bias in the model prediction for the enclosed mass i.e. this term accounts for inaccuracies in the enclosed mass prediction. We note that for a given lens galaxy sample, B will be a function of lens redshift as well as R i.e. $B = B(z_l, R)$.

We can also write B in terms of systematic bias on the galaxy-matter correlation function prediction, $\xi_{\text{gm}}^{\text{bias}}(r) \equiv \xi_{\text{gm}}^{\text{model}}(r) - \xi_{\text{gm}}^{\text{true}}(r)$ i.e. the difference between our model for $\xi_{\text{gm}}(r)$ and the truth,

$$B = \frac{2}{R^2 \Sigma_{\text{crit}}} \int_{-\infty}^{\infty} d\Pi \int_0^R R' dR' \left[1 + \xi_{\text{gm}}^{\text{bias}} \left(\sqrt{R^2 + \Pi^2} \right) \right]. \quad (9)$$

A prior on B could then be constructed from a scale-dependent prior on $\xi_{\text{gm}}^{\text{bias}}(r)$ (see e.g. Baldauf et al. 2016 for more discussion of the inclusion of such theoretical uncertainties in cosmological parameter estimation).

In Section 2.5, we perform tests of our formalism using the $\Delta\Sigma(R)$ signal from a truncated NFW profile (see that section for details). The blue solid lines in Figure 1 shows $\Sigma(R)$ (top-panel) and $\Delta\Sigma(R)$ for a truncated NFW profile, as well as these same quantities for a point-mass with the same total mass as the truncated NFW profile (orange-dashed lines). For the point-mass case, $\Sigma(R)$ is simply a delta function at $R = 0$, while $\Delta\Sigma(R) \propto 1/R^2$. This plot demonstrates the point that 1-halo contributions with very different scale dependence in $\xi_{\text{gm}}(r)$ and therefore $\Sigma(R)$ have very similar scale dependence in $\Delta\Sigma(R)$ on all but the smallest scales. This is why marginalizing over a point-mass contribution can effectively account for an uncertain one-halo contribution.

Of course, by marginalizing over B we lose some information, which will result in a loss in constraining power. However, we believe this is well justified, since the physical scales informing our model are now well-controlled. Assuming that biases in the $\xi_{\text{gm}}(r)$ prediction increase at smaller physical scales, accounting for the non-local contribution in this way should allow for the robust use of smaller scales in the measurement than if the non-local contribution is ignored. As discussed above, if one does have a motivated prior on the potential size of biases in $\xi_{\text{gm}}(r)$ at small scales, that information can be naturally included, and the loss in constraining power will be reduced.

2.2 Analytic marginalization of the enclosed mass contribution

We have described in Section 2.1 how uncertainty in the model prediction for $\Delta\Sigma(R > r_{\text{min}})$ that arises from uncertainty in the model prediction for $\xi_{\text{gm}}(r < r_{\text{min}})$ can be accounted for by marginalizing over a term with $1/R^2$ dependence (equation 7). The simple form of this contamination model (e.g. the scale dependence is not dependent on cosmology or the lens galaxy properties) makes this term suitable for an analytic marginalization approach (see e.g. Bridle et al. 2002). The likelihood desired for our parameter estimation is $P(\Delta\Sigma^{\text{obs}}(R) | \Delta\Sigma^{\text{model}}(R))$ where, as in equation 7, $\Delta\Sigma(R)^{\text{model}}$ is the prediction based on a model for $\xi_{\text{gm}}(r)$ that

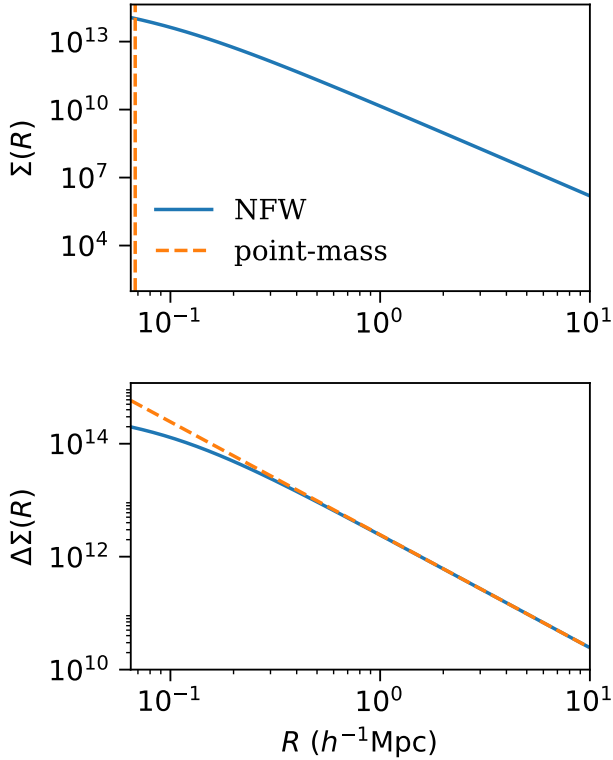


Figure 1. The surface mass density $\Sigma(R)$ (top panel) and surface mass density contrast $\Delta\Sigma(R)$ (bottom panel) for a smoothly truncated NFW halo (blue solid lines, see Section 2.5 for details) and a point-mass of the same mass (orange dashed lines). While the two cases have very different $\Sigma(R)$, they have very similar $\Delta\Sigma(R)$ except at very small scales. Note that in the point-mass case $\Sigma(R)$ is non-zero only at $R = 0$; this is represented in the upper-panel by a vertical line at the left edge of the plot.

is correct only for scales $r > r_{\min}$. This likelihood must be marginalized over the unknown constant B , via

$$P(\Delta\Sigma^{\text{obs}}(R)|\Delta\Sigma^{\text{model}}(R)) = \int dB P(\Delta\Sigma^{\text{obs}}(R)|\Delta\Sigma^{\text{model}}(R), B). \quad (10)$$

In the case that $\Delta\Sigma^{\text{obs}}(R)$ is Gaussian distributed with covariance matrix \mathbf{C} , and we have a Gaussian prior on B with mean zero and width σ_B , one can show that (Bridle et al. 2002) $P(\Delta\Sigma^{\text{obs}}(R)|\Delta\Sigma^{\text{model}}(R))$ is also Gaussian distributed with covariance matrix

$$\mathbf{N} = \mathbf{C} + \sigma_B^2 \vec{x}\vec{x}^T \quad (11)$$

where \vec{x} has elements $x_a = (r_{\min}/R_a)^2$.

This powerful result means that operationally, in order to marginalize over the free parameter B , we need only perform this simple operation on the original covariance matrix \mathbf{C} , rather than explicitly sampling over possible values of B in e.g. an MCMC chain.

In the case that we want to use an “uninformative” or very wide prior on B (i.e. very large σ_B), \mathbf{N} may become close to singular, which will be problematic when numerically calculating \mathbf{N}^{-1} which is required to compute the Gaussian likelihood. We can circumvent this issue by using the

Shermann-Morrison formula to directly calculate \mathbf{N}^{-1}

$$\mathbf{N}^{-1} = (\mathbf{C} + \sigma_B^2 \vec{x}\vec{x}^T)^{-1} \quad (12)$$

$$= \mathbf{C}^{-1} - \frac{\mathbf{C}^{-1} \vec{x}\vec{x}^T \mathbf{C}^{-1}}{\vec{x}^T \mathbf{C}^{-1} \vec{x} + \sigma_B^{-2}}. \quad (13)$$

Indeed with this form we can even use an infinitely wide Gaussian prior on B by taking the limit $\lim \sigma_B \rightarrow \infty$ in which case

$$\mathbf{N}^{-1} = \mathbf{C}^{-1} - \frac{\mathbf{C}^{-1} \vec{x}\vec{x}^T \mathbf{C}^{-1}}{\vec{x}^T \mathbf{C}^{-1} \vec{x}} \quad (14)$$

2.3 Relation to ADSD $\Upsilon(R)$

Baldauf et al. (2010) introduced the Annular Differential Surface Density (ADSD) statistic which they label $\Upsilon(R)$, defined

$$\Upsilon(R; r_{\min}) = \Delta\Sigma(R) - \frac{r_{\min}^2}{R^2} \Delta\Sigma(r_{\min}). \quad (15)$$

This statistic removes the contribution from $R < r_{\min}$ by effectively using the measured signal at r_{\min} to estimate the non-local contribution. We can see this by substituting equation 7 into equation 15, and observing that terms containing B cancel:

$$\Upsilon(R; r_{\min}) = \Delta\Sigma^{\text{model}}(R) + B/R^2 \quad (16)$$

$$- \frac{r_{\min}^2}{R^2} \left[\Delta\Sigma^{\text{model}}(r_{\min}) + B/r_{\min}^2 \right] \quad (17)$$

$$= \Delta\Sigma^{\text{model}}(R) - \frac{r_{\min}^2}{R^2} \Delta\Sigma^{\text{model}}(r_{\min}) \quad (18)$$

We demonstrate in Section 2.5.1 that this approach has very similar performance to marginalizing over the non-local contribution with infinite prior. Which approach is preferred will likely depend on the details of the analysis. As described in Baldauf et al. (2010), a nice feature of the $\Upsilon(R)$ statistic is that it is estimator based, and does not require the introduction of a new free parameter.

Explicitly marginalizing over the point-mass contribution as in our approach (while using analytic marginalization to avoid extra computational cost) allows one to more naturally include a prior, which may allow one to retain more information. We also show that our point-mass marginalization approach can naturally be extended to tomographic measurements where shear-ratio information can be retained, as described in Section 2.4.1.

2.4 Extension to $\gamma_t(\theta)$

Particularly for photometric lens galaxy samples, $\gamma_t(\theta)$ can be a more convenient observable to use than $\Delta\Sigma(R)$ (and in fact the latter is not a direct observable since a cosmological model must be assumed to calculate R from the angular separation). In the flat-sky and Limber approximations, we can relate $\gamma_t(\theta)$ to $\Delta\Sigma(R)$ by integrating over lens and source redshift distributions, $n_l(z)$ and $n_s(z)$:

$$\gamma_t(\theta) = \int dz_l \int dz_s n_l(z_l) n_s(z_s) \frac{\Delta\Sigma(R = \theta \times D_A(z_l), z_l)}{\Sigma_{\text{crit}}(z_l, z_s)}. \quad (19)$$

The B/R^2 term in equation 7 contributes

$$\begin{aligned}\gamma_t^{\text{pm}}(\theta) &= \int dz_1 \int dz_s n_l(z_1) n_s(z_s) \frac{B(z_1, R = \theta \times D_A(z_1))}{R^2 \Sigma_{\text{crit}}(z_1, z_s)} \\ &= \theta^{-2} \int dz_1 \int dz_s n_l(z_1) n_s(z_s) \frac{B(z_1, R = \theta \times D_A(z_1))}{D_A^2(z_1) \Sigma_{\text{crit}}(z_1, z_s)}.\end{aligned}\quad (20)$$

where $D_A(z_1)$ is the angular diameter distance to the lens redshift z_1 . Note that the bias in the enclosed mass prediction $B(z_1, R)$ can now in general depend on the lens redshift and the radius R corresponding to the angular separation θ at redshift z_1 .

Hence for $\gamma_t(\theta)$, we can similarly remove the impact of modelling inaccuracies in $\xi_{\text{gm}}(r)$ at scale $r < r_{\text{min}}$ by marginalizing over a term with scale dependence $1/\theta^2$, for angular scales $\theta > r_{\text{min}}/D_A(z_{1,\text{min}})$ where $D_A(z_{1,\text{min}})$ is the distance to the lowest redshift lenses considered (i.e. for angular scales corresponding to physical scales greater than r_{min} in the lens plane).

2.4.1 The tomographic case

For photometric surveys it is convenient and, given the limited photometric redshift precision, often close to optimal to perform a *tomographic* analysis where lenses and/or source are split into multiple bins in redshift and correlations between all pairs of lens and source redshift bins are used. In this case, our prediction for the tangential shear for lens bin i , and source bin j is

$$\gamma_{t,ij}(\theta) = \gamma_{t,ij}^{\text{model}}(\theta) + C_{ij}/\theta^2 \quad (22)$$

where

$$C_{ij} = \int dz_1 \int dz_s n_{l,i}(z_1) n_{s,j}(z_s) \frac{B_i(z_1, R = \theta * D_A(z_1))}{D_A^2(z_1) \Sigma_{\text{crit}}(z_1, z_s)}. \quad (23)$$

If the lens redshift distribution is sufficiently narrow, or $B_i(z_1, R)/D_A^2(z_1)$ evolves with redshift sufficiently slowly across the width of the lens redshift bin, then we can make the approximation

$$C_{ij} \approx B_i \int dz_1 dz_s n_{l,i}(z_1) n_{s,j}(z_s) \Sigma_{\text{crit}}^{-1}(z_{1,j}, z_s) D_A^{-2}(z_1) \quad (24)$$

$$\equiv B_i \beta_{ij} \quad (25)$$

i.e. only a single free parameter B_i is required for each lens redshift bin (rather than a free parameter C_{ij} for each lens-source redshift bin pair), with the impact on each lens-source pair modulated by the effective inverse Σ_{crit} , β_{ij} . We'll call this the *narrow lens bin assumption*. Of note here is that if we can make this narrow lens bin assumption, then we can extract shear-ratio information from the enclosed mass term, without any assumption about the amplitude of that mass. In effect, we gain constraining power on the relative sizes of the β_{ij} , which contain geometric information through their dependence on the angular diameter distances which enter Σ_{crit} (see equation 2.1), and thus information on cosmological parameters (e.g. Jain & Taylor 2003; Taylor et al. 2007; Miyatake et al. 2017) and nuisance parameters quantifying e.g. photometric redshift uncertainties (e.g. Heymans et al. 2012; Prat et al. 2018a). We note that one can of course choose the width of the lens redshift bins in order to attempt to satisfy this narrow lens bin assumption. The success of this

approach will depend on whether the lens galaxy redshift uncertainties allow the construction of sufficiently narrow redshift bins.

In the tests below (Section 2.5, Section 4), we do not explore realistic cases of the redshift evolution of $B_i(z_1, R)/D_A^2(z_1)$, which would require realistic galaxy simulations, and is beyond the scope of this work. We instead focus on demonstrating the usefulness of this formalism in idealized cases where the narrow lens bin assumption can be safely assumed.

2.4.2 Analytic marginalisation

In the case that we have n_{lens} lens redshift bins and n_{src} source redshift bins we need a model for the full length- N_d tangential shear vector (i.e. the concatenation of all angular scales for all lens and source redshift bin pairs) $\vec{\gamma}_t = [\vec{\gamma}_{t,00}, \dots, \vec{\gamma}_{t,0n_{\text{src}}}, \dots, \vec{\gamma}_{t,n_{\text{lens}}n_{\text{src}}}]$.

In the case that we can make the narrow lens bin assumption in equation 25, we can use the following form:

$$\gamma_t(\theta) = \gamma_t^{\text{model}}(\theta) + B_i \beta_{ij} \theta^{-2} \quad (26)$$

where i and j are the lens and source redshift, and again $\vec{\gamma}_t^{\text{model}}$ is based on a ξ_{gm} prediction that is accurate only down to some scale r_{min} . It is useful to write this in vector notation:

$$\vec{\gamma}_t = \vec{\gamma}_t^{\text{model}} + \sum_i^{n_{\text{lens}}} B_i \vec{t}_i \quad (27)$$

where

$$(\vec{t}_i)_a = \begin{cases} 0 & \text{if lens redshift bin for element } a \text{ is not } i \\ \beta_{ij} \theta_a^{-2} & \text{otherwise} \end{cases} \quad (28)$$

where j is the source redshift bin and θ_a is the angular separation for element a of the full datavector. We note that in the above, and throughout, we use i and j as redshift bin labels rather than vector indices; \vec{t}_i in equation 26 does not represent element i of a vector \vec{t} , rather one of a set of n_{lens} vectors. When we do provide a piece-wise definition of a vector we use an index a as in equation 28.

Analytic marginalization over all B_i can again be performed by updating the covariance matrix to \mathbf{N} given by

$$\mathbf{N} = \mathbf{C} + \sum_i \sigma_{B_i}^2 \vec{t}_i \vec{t}_i^T \quad (29)$$

where \mathbf{C} is the original γ_t covariance and σ_{B_i} is width of the Gaussian prior on B_i .

We can also write \mathbf{N} in the form

$$\mathbf{N} = \mathbf{C} + \mathbf{U} \mathbf{U}^T \quad (30)$$

where \mathbf{U} is a $N_d \times n_{\text{lens}}$ matrix with i th column $\sigma_{B_i} \vec{t}_i$, and N_d is the number of elements in the datavector. We will refer to \mathbf{U} as a *template matrix* since its columns are template modes to be marginalized over. We can use the Woodbury matrix identity (the generalization of the Sherman-Morrison formula introduced in Section 2.2) to get the inverse:

$$\mathbf{N}^{-1} = \mathbf{C}^{-1} - \mathbf{C}^{-1} \mathbf{U} (\mathbf{I} + \mathbf{U}^T \mathbf{C}^{-1} \mathbf{U})^{-1} \mathbf{U}^T \mathbf{C}^{-1}. \quad (31)$$

where \mathbf{I} is the identity matrix.

Again, we may want to consider the case where we allow maximal freedom in the model by taking the limit $\sigma_{B_i} \rightarrow \infty$. In this case equation 31 reduces to

$$\mathbf{N}^{-1} = \mathbf{C}^{-1} - \mathbf{C}^{-1} \mathbf{V} (\mathbf{V}^T \mathbf{C}^{-1} \mathbf{V})^{-1} \mathbf{V}^T \mathbf{C}^{-1}. \quad (32)$$

where \mathbf{V} is a $N_d \times n_{\text{lens}}$ matrix with i th column \vec{t}_i .

If we cannot make the narrow lens bin assumption, then we have

$$\vec{\gamma}_t = \vec{\gamma}_t^{\text{model}} + \sum_{i=1}^{n_{\text{lens}}} \sum_{j=1}^{n_{\text{src}}} C_{ij} \vec{t}_{ij} \quad (33)$$

where we now use ij to label the lens-source redshift bin pair, and

$$(\vec{t}_{ij})_a = \begin{cases} \theta_a^{-2} & \text{if the lens-source redshift bin pair} \\ & \text{for element } a \text{ is } ij \\ 0 & \text{otherwise} \end{cases} \quad (34)$$

We can again marginalize over the free parameters C_{ij} analytically, transforming the covariance matrix \mathbf{C} according to equation 2.4.2. In this case \mathbf{U} is a $N_d \times N_p$ matrix, where $N_p = n_{\text{lens}} \times n_{\text{src}}$, the total number of lens-source redshift bin pairs. The p th column (where $p = i \times n_{\text{lens}} + j$) is given by $\sigma_{C_{ij}} \vec{t}_{ij}$ where $\sigma_{C_{ij}}$ is the width of the Gaussian prior on C_{ij} .

2.5 Simple Tests

In this section we test the the above formalism by using it in parameter estimation on galaxy-galaxy lensing datavectors with reasonable one-halo contamination. For all tests where we use analytic marginalization we use the infinite prior case. For the point-mass marginalization, this means we make no assumption about $\xi_{\text{gm}}(r)$ below r_{min} .

We first describe our simulated datavector, which is used here and in Section 4. We generate a galaxy-galaxy lensing and galaxy clustering datavector based on that used in the DES Year 1 analyses of Krause et al. (2017); DES Collaboration et al. (2017). The galaxy clustering part of the datavector is not used in this section, but is used in Section 4. The lens sample has 5 redshift bins spanning a range of 0.15 – 0.9 in redshift. The source sample has 4 redshift bins, roughly spanning a range 0.2 – 1.3 in redshift (see Figure 1 of DES Collaboration et al. (2017) for more details). Both galaxy-galaxy lensing and galaxy clustering signals are generated according to a linear bias model, with values of the galaxy bias, $b_i = [1.45, 1.55, 1.65, 1.8, 2.0]$. Simulated measurements are generated for 20 log-spaced bins between angular scales 2.5 and 250 arcminutes. Again following DES Collaboration et al. (2017); Krause et al. (2017), in our linear bias model the galaxy-galaxy and galaxy-matter power spectra for redshift bin i are in fact generated as $P_{\text{gg}} = (b_i)^2 P_{\text{nl}}$ and $P_{\text{gm}} = b_i P_{\text{nl}}$, where P_{nl} is the nonlinear matter power spectrum calculated using HALOFIT (Smith et al. 2003; Takahashi et al. 2012). Throughout, we use the COSMOSIS⁴ package (Zuntz et al. 2015) for theory predictions and parameter inference, implementing in custom modules the 1-halo contamination and Gaussian covariance calculation described below, as well as our analytic marginalization scheme.

We generate a Gaussian covariance matrix corresponding to this datavector which has roughly DES Year 5 statistical power - we assume an area of 5000 deg², a lens galaxy number density of [0.013, 0.034, 0.051, 0.030, 0.0088] galaxies per square arcminute, a source galaxy number density of 2 per square arcminute for each redshift bin (i.e. totalling 8 source galaxies per square arcminute), and $\sigma_e = 0.4$ (the total ellipticity dispersion) for all source redshift bins.

We add to the galaxy-galaxy lensing simulated datavector a simple 1-halo contribution (on top of the linear bias term already present). For each lens redshift bin, based on the fiducial linear bias values above, and the mean redshift of the bin, we calculate a fiducial halo mass M_{200} value following Tinker et al. (2010) and concentration, c following Duffy et al. (2008). The 1-halo contribution is then calculated as the tangential shear from a truncated NFW profile with mass M_{200} and concentration c at the mean redshift of the lens redshift bin only - meaning we can safely make the narrow lens assumption for this contamination term. For convenience, we use the smoothly truncated NFW density profile in Equation A.3 of Baltz et al. (2009), with $\tau = 2$, since this allows for analytic calculation of $\Delta\Sigma(R)$.

We note that our model for the galaxy-matter correlation function, which is the sum of a linear bias 2-halo contribution, and a one-halo term, is not very realistic. We do not include satellite galaxies in the model, or a realistic distribution of halo mass and concentration. It is unlikely to be accurate in the *transition* regime, where the one and two-halo contributions are of comparable size. Additionally, our 2-halo term does not have a cut-off at small scales to account for halo exclusion (e.g. Smith et al. 2007) so may make too large a contribution here. We stress that this model, while of limited realism, is well-suited to demonstrate the usefulness of the techniques presented here, where we marginalize over the impact of the 1-halo contribution without making assumptions about its functional form or even amplitude. We defer the study of more realistic one-halo contamination to future work using galaxy simulations, focusing here instead on proof-of-concept type tests.

Unless otherwise stated, we throughout impose minimum angular scales in our simulated datavector corresponding to $4 h^{-1}$ Mpc at the mean redshift of the lens redshift bin, which equate to [21.5, 13.5, 10.0, 8.0, 7.0] arcminutes for the five lens redshift bins.

2.5.1 Recovering the linear galaxy bias from $\gamma_t(\theta)$

As a first simple step we test the recovery of the linear bias, b_i for each lens redshift bin i , from the galaxy-galaxy lensing signal only. We fix all other parameters fixed and analyse the datavector with and without using our analytic marginalization scheme to account for the 1-halo contamination. The solid markers in Figure 2 shows the bias in the recovered b_i , calculated as $\langle b_i \rangle - b_{i,\text{true}}$ where $\langle b_i \rangle$ is the mean of the marginalized posterior and $b_{i,\text{true}}$ is the galaxy bias value used to generate the datavector. For the blue circles marginalization over the point-mass contribution was not performed, and hence biased values for the galaxy bias are recovered, while for the orange markers point-mass marginalization was included, and the correct galaxy bias values are recovered. The corresponding open markers indicate the 1σ uncertainty on the recovered linear bias parameter, demon-

⁴ <https://bitbucket.org/joezuntz/cosmosis/>

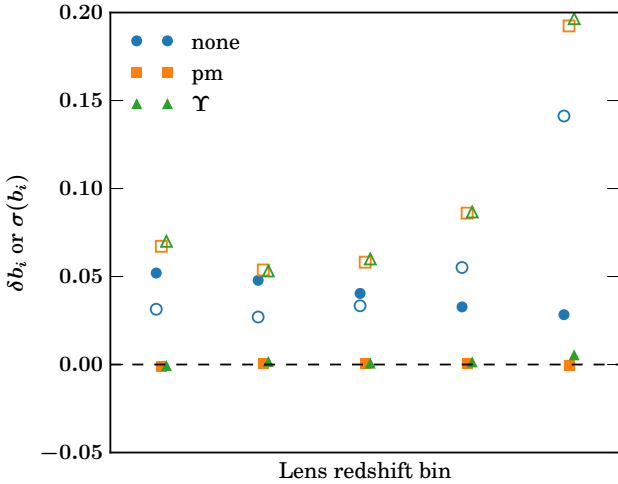


Figure 2. The bias (filled markers) and $1-\sigma$ uncertainty (unfilled markers) on the inferred linear galaxy bias values from a DES-like galaxy-galaxy lensing datavector with five lens redshift bins (described in Section 2.5) at fixed cosmology. The blue markers show the case where no marginalization is performed to account for the 1-halo contribution and hence the recovered values are somewhat biased. The orange markers show the case where the analytic marginalization scheme in Section 2.4.2 is used. Green markers use the ADSD statistic and recover essentially the same constraints as the point-mass marginalization approach.

strating that as expected, there is some degradation in constraining power when using the point-mass marginalization scheme.

We also implement the analogous ADSD statistic for $\gamma_t(\theta)$,

$$\Upsilon(\theta) = \gamma_t(\theta) - \left(\frac{\theta}{\theta_{\min}}\right)^2 \gamma_t(\theta_{\min}). \quad (35)$$

This shows very similar performance to the point-mass marginalization approach. For simplicity, we use as $\gamma_t(\theta_{\min})$ simply the smallest angular bin in the measurement remaining after applying the scale cuts. When the ADSD statistic has been used on data, an estimate of $\Delta\Sigma(r_{\min})$ has typically been made by fitting a power-law over a range of scales around r_{\min} (e.g. Mandelbaum et al. 2013). We do not attempt to compare to this more complex approach here, although we note that analogous information could be added to the point-mass marginalization.

2.5.2 Shear-ratio information

As described in Section 2.4.1, if we make the narrow lens bin assumption we can straightforwardly retain the shear-ratio information in the point-mass term. One way to demonstrate this is to allow some freedom in the redshift distributions of the source redshift distributions, and test our constraining power on these distributions. Shear-ratio measurements have already been used for this application by Prat et al. (2018b) who extracted competitive constraints on these shift parameters using DES Year 1 galaxy-galaxy lensing measurements. Using the same contaminated galaxy-galaxy lensing datavector described above, we allow a simple shift δz_j for source

redshift bin j . For this test we keep the linear bias and cosmological parameters fixed to their true values. We produce constraints on the δz_j with three different modeling approaches, introduced here with the same labelling used in Figure 3:

(i) ‘none’: we do not marginalize over the point-mass contribution and hence expect this approach to produce the tightest, but also biased constraints.

(ii) ‘pm w/o Σ_{crit} ’: we analytically marginalize over the point-mass contribution but allow a fully independent contribution for each lens-source redshift bin pair (following equation 33, thereby not retaining shear-ratio information from the point-mass contribution.

(iii) ‘pm’: we analytically marginalise over an independent point-mass contribution for each lens redshift bin i.e. assume a perfectly correlated contribution to all source redshift bins for a given lens bin (following equation 27).

Figure 3 shows the mean of the posterior on δz_j (solid markers, solid lines) and its $1-\sigma$ uncertainty (open markers, dashed lines) for the three cases above (blue circles, orange squares, and green triangles respectively). We see again that there is a degradation in constraining power when performing the point-mass marginalization with either method (ii) or (iii), but that this degradation is smaller for the case (iii) where shear-ratio information in the point-mass contribution is retained, particularly for the two lower source redshift bins.

3 MAKING USE OF ALL MEASURED SCALES IN THE TANGENTIAL SHEAR

We can extend the above formalism to make use of all measured scales in our $\gamma_t(\theta)$ measurement. As above, we assume that for each lens redshift bin, i , there is an angular scale θ_{\min}^i which corresponds to a physical scale in the lens plane r_{\min} , below which we do not have a trustworthy model for the galaxy-matter correlation function $\xi_{\text{gm}}(r)$. We therefore cannot make a reliable model prediction for $\gamma_t(\theta < \theta_{\min}^i)$ (even if a point-mass contribution were marginalized over). However if we can make the narrow lens redshift bin assumption, we do know how the relative amplitudes of the different lens-source bin combinations for a given lens redshift bin are related i.e.

$$\gamma_{t,ij}(\theta < \theta_{\min}^i) / \gamma_{t,i'j'}(\theta < \theta_{\min}^i) = \beta_{ij} / \beta_{i'j'}. \quad (36)$$

For any measured scale we can therefore write down our model for lens redshift bin i and source redshift bin j as:

$$\gamma_{t,ij}(\theta) = \gamma_{t,ij}^{\text{model}}(\theta) + \beta_{ij} B_i / \theta^2 + \beta_{ij} D_i(\theta). \quad (37)$$

The second term is the point-mass contribution described in Section 2 and is not included for scales $\theta < \theta_{\min}^i$. We have now added a third term containing a function $D_i(\theta)$ that is zero for $\theta > \theta_{\min}^i$, and allowed to vary freely for scales $\theta < \theta_{\min}^i$. Physically, for $\theta < \theta_{\min}^i$ we are allowing the value of $\Delta\Sigma(R = \theta D_l)$ to vary freely for $\theta < \theta_{\min}^i$, while enforcing that it takes the same value for a given angular scale and lens redshift bin, and hence is simply modulated in $\gamma_{t,ij}$ by β_{ij} . We refer to marginalization over the $D_i(\theta)$ as *small-scale marginalization*.

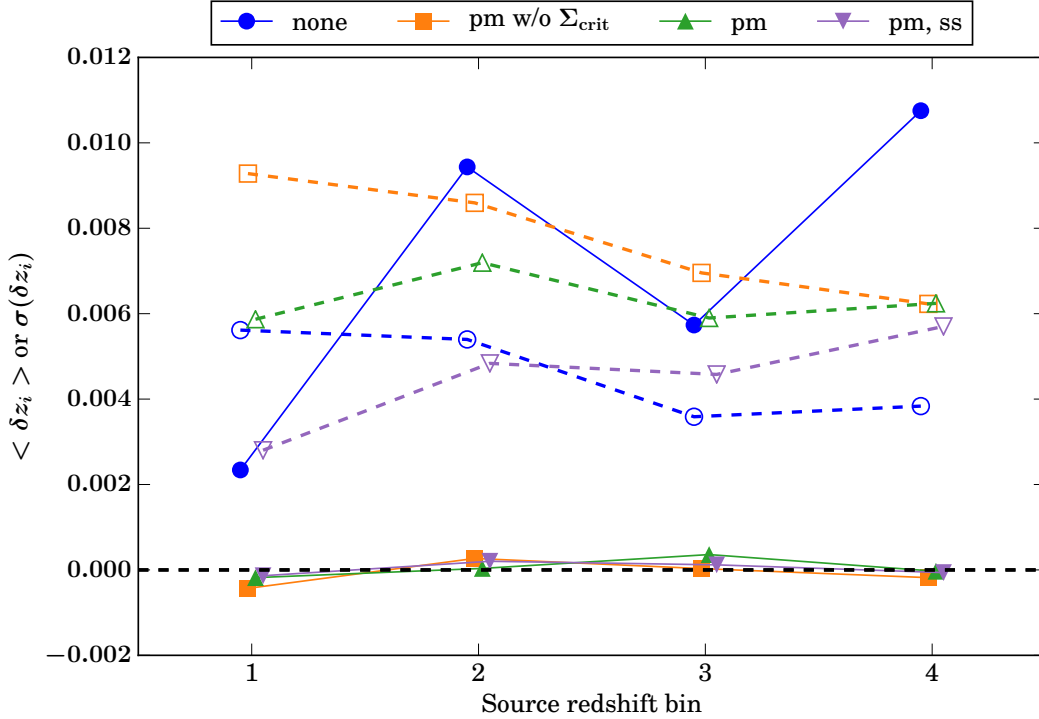


Figure 3. The bias (filled markers, solid lines) and uncertainty (unfilled markers, dashed lines) on the inferred value of δz_i , the shift in the redshift distribution for source redshift bin j , for different small scale $\gamma_l(\theta)$ treatments. The datavector is based on a DES Year 1 galaxy-galaxy lensing datavector with DES Year 5-like uncertainties. ‘none’ indicates no point-mass marginalization is performed and small-scales are removed. ‘pm w/o Σ_{crit} ’ indicates point-mass marginalization is performed for each lens-source redshift bin pair independently (i.e. no shear-ratio relation is assumed). ‘pm’ indicates point-mass marginalization is performed for each lens redshift bin independently, retaining shear-ratio information. ‘pm, ss’ indicates both point-mass marginalization and small-scale marginalization are performed, the approach that retains the most information while still being unbiased.

One may ask if we are introducing too much freedom in the model, since the point-mass contribution at large scales is determined by the density profile at small scales, which we are also now marginalizing over. However, the density profile is never fully determined down to zero, since the shape noise on the measurement diverges in the limit of zero angular separation. Using some parameterization for the projected density profile down to zero would allow the information from these small scales to constrain the point-mass contribution to larger scales, potentially reducing degradation in the constraints when marginalizing over the point-mass term. We leave further investigation of this approach for future work.

Analytic marginalization is again extremely useful here, since we may want to marginalize over 10s or 100s of $D_i(\theta)$ values. In order to perform analytic marginalization, it is again useful to recast in vector notation, with the full $\gamma_l(\theta)$ datavector given by

$$\vec{\gamma}_l = \vec{\gamma}_l^{\text{model}} + \sum_i^{n_{\text{lens}}} B_i \vec{t}_i + \sum_i^{n_{\text{lens}}} \sum_k^{N_{\theta}^i} D_{ik} \vec{s}_{ik} \quad (38)$$

where N_{θ}^i is the number of angular bins for lens bin i with $\theta < \theta_{\text{min}}^i$, and

$$(\vec{s}_{ik})_a = \begin{cases} \beta_{ij} \Theta(\theta_a, \theta_{\text{min}}^i) & \text{if lens redshift bin and angular bin} \\ & \text{for element } a \text{ are } i \text{ and } k \text{ respectively} \\ 0 & \text{otherwise} \end{cases}$$

(39)

where j is the source redshift bin for datavector element a and

$$\Theta(X, Y) = \begin{cases} 1 & \text{if } X < Y \\ 0 & \text{otherwise.} \end{cases} \quad (40)$$

We also update the definition of \vec{t}_i such that the point-mass contribution is not marginalized over for scales $\theta < \theta_{\text{min}}^i$:

$$(\vec{t}_i)_a = \begin{cases} 0 & \text{if lens redshift bin for element } a \text{ is not } i \\ \beta_{ij} \theta_a^{-2} \Theta(\theta_{\text{min}}^i, \theta_a) & \text{otherwise} \end{cases} \quad (41)$$

The D_{ik} in equation 38 are the set of free parameters we introduce to marginalize over the density profile at small scales. We note again that i, j and k in the above are not vector or tensor indices, but rather labels for lens redshift bin and angular bin respectively i.e. D_{ik} and s_{ik} are from sets of $\sum_i^{n_{\text{lens}}} N_{\theta}^i$ scalars and vectors respectively. As in the case of the point-mass contribution, we can perform this marginalization analytically by updating the $\gamma_l(\theta)$ covariance matrix according to equation 2.4.2, where now $\mathbf{U} = (\mathbf{U}_{\text{pm}} | \mathbf{U}_{\text{ss}})$, the concatenation of the template matrices for the point-mass marginalization and the small-scale marginalization over the $D_i(\theta)$ described in this section. \mathbf{U}_{ss} is a matrix with dimensions $N_d \times N_q$, where $N_q = \sum_i^{n_{\text{lens}}} N_{\theta}^i$, the total number of dat-

apoints with $\theta < \theta_{\min}^i$. It has columns $\sigma_{D_{ik}} \vec{s}_{ik}$ where $\sigma_{D_{ik}}$ is the Gaussian prior width for the free parameter D_{ik} .

We repeat the test in Section 2.5.2 in which we analyse a $\gamma_t(\theta)$ datavector, which contains unmodelled contamination by a 1-halo term, while allowing shifts in the source bin redshift distributions δz_j . To increase the usefulness of the small-scale marginalization described here, we extend the simulated measurements down to smaller scales - adding another 10 logspaced angular bins between 0.25 and 2.5 arcminutes. When not using the small-scale marginalization scheme, these extra scales are removed by the scale cuts, so have no bearing.

The results are again plotted in Figure 3. The purple downwards facing triangles represent the case where both point-mass and small-scale marginalization are used. Compared to the ‘‘pm’’ case where only point-mass marginalization is used, the inferred δz_i values remain unbiased, but uncertainties are significantly reduced. In the two lowest redshift bins, the extra information reduces statistical uncertainties to below those in the ‘‘none’’ (no point-mass or small-scale marginalization) case. We conclude that this double-pronged approach of marginalization over both the point-mass contribution, and the underlying signal at too-small-to-model scales, is the most successful at recovering unbiased shear-ratio information.

4 TESTS OF COSMOLOGICAL PARAMETER ESTIMATION

We perform some simple simulated-likelihood tests to show how our analytic marginalization scheme helps with unbiased cosmological inference. We simulate parameter estimation on the joint galaxy-galaxy lensing and galaxy clustering datavector described in Section 2.5. For each lens redshift bin i , we again cut out angular scales less than θ_{\min}^i corresponding to $< 4 h^{-1}$ Mpc in the lens plane for both the galaxy-galaxy lensing and clustering measurements, except in the case that we retain these scales for the small-scale marginalization scheme described in Section 3. In this case angular scales less than θ_{\min}^i are retained in galaxy-galaxy lensing only, and are only used for the small-scale marginalization scheme, rather than being modeled explicitly.

We analyse the datavector (again using the DES Year 5-like covariance) with three modelling approaches:

- (i) No marginalization (point-mass or small-scale) is performed
- (ii) only point-mass marginalization is performed
- (iii) both point-mass and small-scale marginalization are performed

Firstly, we vary only a linear bias parameter for each lens redshift bin, the matter density, Ω_m in the range [0.1, 0.9], the amplitude of the primordial power spectrum, A_s in the range [0.5×10^{-9} , 5×10^{-9}] and h in the range [0.4, 0.95] (with the Hubble constant given by $H_0 = 100 h$ (km/s)/Mpc). We assume a flat Λ CDM cosmology with all other cosmological parameters fixed. σ_8 is recorded in our MCMC chains as a derived parameter. For our fiducial setup, the resulting constraints on Ω_m and $S_8 = \sigma_8(\Omega_m/0.3)^{0.5}$ are shown in the top-left panel of Figure 4 (here and throughout, contours represent the 68% and 95% credible intervals).

As expected, modelling approach (i) results in the tightest, but biased constraints, since potential contamination by the 1-halo term is not marginalized over. Cases (ii) and (iii) recover the true cosmology (indicated by the dashed lines) correctly. For this parameter space there is a modest gain in constraining power when using the small-scale marginalization (i.e. the gain in case (iii) over case (ii)), with a 16% decrease in the uncertainty on Ω_m .

In the other three panels of Figure 4, we study how the different modeling approaches perform under variations to our fiducial setup. The top-right and bottom-left panels use larger and smaller minimum scales in both galaxy-galaxy lensing and clustering (corresponding to $8 h^{-1}$ Mpc and $2 h^{-1}$ Mpc in the lens plane), with a couple of trends becoming apparent. Firstly, when using smaller scales, the bias when not performing point-mass marginalization (the contour labelled ‘none’) is increased in significance. Secondly, when using smaller scales, the gain from using the small-scale marginalization relative to point-mass marginalization only is reduced (this is expected since there is simply less information for the small-scale marginalization to reclaim).

Finally, in the bottom-right panel, we re-compute the covariance matrix with four times the density of source galaxies (keeping our fiducial scale cuts). This is potentially useful to gain an intuition on how the results here may apply to other lensing surveys which have a higher source galaxy density than DES, like the Hyper Suprime-Cam Subaru Strategic Survey⁵ (HSC, Mandelbaum et al. 2018), LSST or WFIRST. Increasing the source galaxy number density decreases the shape noise on the galaxy-galaxy lensing measurement, which is the dominant contributor to the covariance on small scales. This makes the bias in inferred parameters when no point-mass marginalization is performed (the ‘none’ case) more significant than in the fiducial case. The extra signal-to-noise on small scales also leads to a greater gain in constraining power when using small-scale marginalization compared to point-mass marginalization only, with the $1 - \sigma$ uncertainty on Ω_m reduced by 23%.

An impression one may take from Figure 4 is that the decrease in constraining power when using the point-mass marginalization (orange and green outlined contours) is rather large compared to the parameter bias when not using it (blue solid contour). We note that the size of this bias here is a direct result of the highly simplified, order-of-magnitude model we’ve chosen for inaccuracy in the $\xi_{\text{gm}}(r)$ model (contamination by a simple 1-halo term), our chosen scale cuts (e.g. using smaller scales would result in greater bias), and survey properties. In reality, for a given galaxy sample and observational setup, biases could be much larger or smaller. Furthermore, unlike in the test presented here, one would be unlikely to use the same minimum scale cut in the two approaches - a more conservative minimum scale would likely be required when not marginalizing over the point-mass to meet some requirement on the ratio between inferred parameter bias and uncertainty. We further note that informative priors on the point-mass contribution can be naturally included in our framework and would reduce the degradation when including the point-mass marginalization.

Next, (returning to our fiducial scale cuts and source

⁵ <https://hsc.mtk.nao.ac.jp/ssp/>

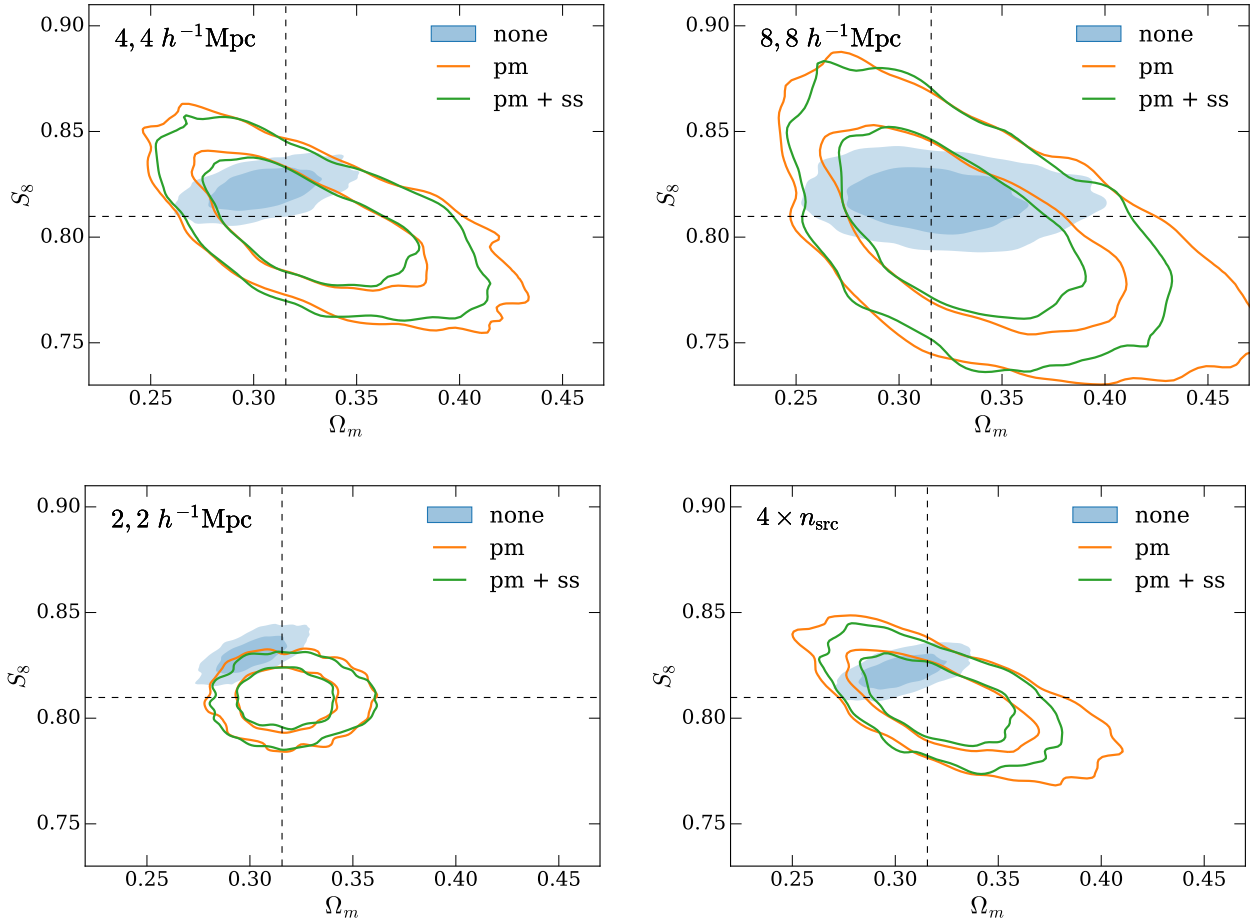


Figure 4. All panels show constraints on Ω_m and $S_8 = \sigma_8(\Omega_m/0.3)^{0.5}$ for a DES-like galaxy-galaxy lensing and galaxy clustering analysis. The simulated datavector has contamination by an un-modeled one-halo term in the galaxy-galaxy lensing signal (described in Section 2.5). In addition to Ω_m and σ_8 , the Hubble constant H_0 , and a linear bias for each redshift bin are varied (see Section 4 for details). The true values (i.e. those used to generate the datavector) are shown as the grey dashed lines. The three sets of contours represent the three modeling approaches described in Section 4. Blue solid contours result from using neither point-mass or small-scale marginalization. The orange outlined contours use point-mass but not small-scale marginalization. The green outlined contours use both point-mass and small-scale marginalization. The top-left panel is for our fiducial setup described in Section 2.5. In the top-right (bottom-left) panels we use larger (smaller) minimum scale cuts corresponding to $8 h^{-1}\text{Mpc}$ ($2 h^{-1}\text{Mpc}$) in the lens plane for both galaxy-galaxy lensing and clustering. In the bottom-right panel, a source galaxy number density 4 times higher than the fiducial setup is assumed.

galaxy density) we additionally allow w_0 , the (constant with redshift) dark energy equation of state parameter, to vary from its ΛCDM value of -1 , in the range $[-3, -0.33]$. Figure 5 shows marginalized constraints on Ω_m , S_8 , h and w_0 . Again, modeling approach (i) recovers the tightest constraints, but biases with respect to the truth values are present, with the truth lying outside the 68% credible interval in the $S_8 - h$ and $S_8 - \Omega_m$ planes for example. Again, when using small-scale marginalization, modest gains in constraining power are apparent in most of the 2d projections of the posterior, and the constraint on w_0 is improved by 16% with respect to the case when only point-mass marginalization is used.

5 DISCUSSION

We have described and demonstrated a methodology which uses an analytic marginalization approach to target two is-

suues with small scale galaxy-galaxy lensing measurements. Firstly, the galaxy-galaxy lensing signal measured at physical separation R in the lens plane receives significant contributions from scales $r < R$ in the galaxy-matter correlation function $\xi_{\text{gm}}(r)$. We have described how uncertainty in the model prediction for this contribution can be straightforwardly marginalized over by including in the model a $1/R^2$ (for $\Delta\Sigma(R)$) or $1/\theta^2$ (for $\gamma_t(\theta)$) dependence with free amplitude. We demonstrate that this approach can successfully remove biases in inferred parameters when an un-modeled one-halo contribution is present in the galaxy-galaxy lensing signal, and that this marginalization can be performed analytically, to avoid adding extra sampling parameters to the parameter inference. We note that the approach of Baldauf et al. (2010) also achieves this goal, although our approach may more naturally allow the use of priors and retention of shear-ratio information in a tomographic analysis.

Secondly, we demonstrate that an analytic marginaliza-

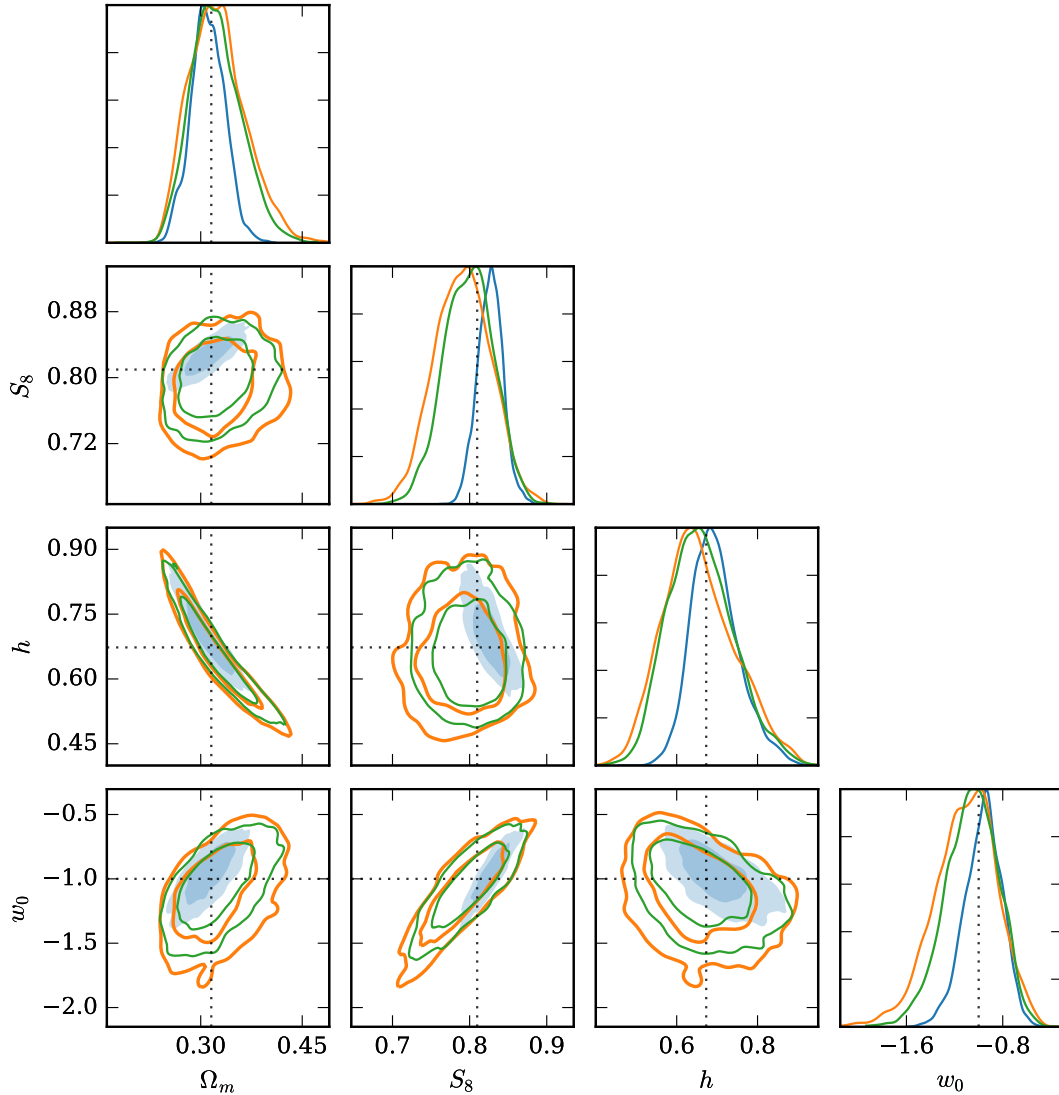


Figure 5. Simulated constraints on cosmological parameters from a DES Year 5-like galaxy-galaxy lensing and galaxy clustering analysis (see Section 4 for details). The simulated datavector has contamination by an un-modeled one-halo term in the galaxy-galaxy lensing signal (described in Section 2.5). All varied cosmological parameters are shown. A linear bias parameter for each lens redshift bin is also marginalized over. The true values (i.e. those used to generate the datavector) are shown as the grey dotted lines. The three sets of contours represent the three modeling approaches described in Section 4. Blue solid contours result from using neither point-mass or small-scale marginalization. The orange outlined contours use point-mass but not small-scale marginalization. The green outlined contours use both point-mass and small-scale marginalization.

tion approach can also be used to extract shear-ratio information from small scale galaxy-galaxy lensing measurements that would otherwise be excluded due to modelling uncertainties i.e. those corresponding to physical separation in the lens plane $R < r_{\min}$, where r_{\min} is the smallest physical scale for which a $\xi_{\text{gm}}(r)$ prediction is accurate. Again, the use of analytic marginalization allows us include many extra nuisance parameters without having to explicitly sample over them in a Monte Carlo chain, making the approach tractable for cosmological parameter estimation. We have shown that this extra shear-ratio information allows improved constraints on parameters which account for

photometric redshift uncertainties, as well as cosmological parameters. Our approach here is an example of including theoretical uncertainties in the model, which is explored in detail by Baldauf et al. (2016). Our case is an extreme one in that we allow complete freedom in $\Delta\Sigma$ below some scale.

When it comes to using such methodology in an analysis of real data, there are several factors to consider that merit some discussion. Firstly, when using the point-mass marginalization, one must still choose a minimum scale r_{\min} for which the $\xi_{\text{gm}}(r)$ prediction is trustworthy. We have discussed the rough scales on which typical modeling approaches are likely to break down at a level relevant to cur-

rent and future large-scale structure surveys: $\sim 10 - 20$ Mpc for a linear bias model, a few megaparsecs for a higher-order perturbative approach, while an HOD approach could potentially be reliable to tens or hundreds of kiloparsecs.

Ultimately, realistic, large volume galaxy simulations are required to inform this decision. Cosmological hydrodynamical simulations, which attempt to include some of the hydrodynamical processes important for galaxy formation, have advanced significantly in the past decade both in terms of simulation volume, and matching observed properties of the real universe (e.g. [Schaye et al. 2010](#); [Vogelsberger et al. 2014](#); [Schaye et al. 2015](#); [Springel et al. 2018](#)). However, there is still much uncertainty in the sub-grid prescriptions required to implement physical processes on scales below the resolution of these simulations. While uncertainty in the sub-grid modelling may not strongly impact the mass distribution on larger scales, it will impact the dependence of observable galaxy properties on that mass distribution, and hence the galaxy-galaxy lensing and clustering signals of a galaxy sample selected on observable properties.

It is likely therefore that empirical approaches where galaxies are added to gravity-only simulations using recipes calibrated against cosmological observables (e.g. [Tasitsiomi et al. 2004](#); [Conroy et al. 2006](#); [Hearin et al. 2014](#); [Crocce et al. 2015](#); [DeRose et al. 2019](#)) will continue to play an important role in understanding the relation between the distributions of galaxies and the distribution of matter in the Universe (see [Wechsler & Tinker \(2018\)](#) for a recent review).

Such simulations are also likely required to estimate the impact of redshift evolution of lens properties across the width of lens redshift bins, a potential systematic effect when extracting shear-ratio information using the methods presented here. We are hopeful however that given that galaxy-galaxy lensing analyses have typically been performed using lens galaxies with spectroscopic or high quality photometric redshifts, sufficiently narrow lens bins could usually be constructed.

Finally, we note the potential problems due to intrinsic galaxy alignments. If photometric redshift uncertainties in the source galaxy sample allow some overlap in redshift between the lens and source samples, there may be some net alignment of source galaxies' intrinsic shapes around lens galaxy positions ([Hirata et al. 2004](#); [Troxel & Ishak 2014](#); [Joachimi et al. 2015](#); [Blazek et al. 2012](#)). Significant contamination from intrinsic alignments could bias the shear-ratio information extracted from small-scale galaxy-galaxy lensing signals, since the intrinsic alignment contribution will not scale according to equation 3. So far, detections of this intrinsic alignment signal have largely been limited to bright, red galaxies (e.g. [Mandelbaum et al. 2006](#); [Hirata et al. 2007](#); [Joachimi et al. 2011](#); [Blazek et al. 2011](#); [Singh & Mandelbaum 2016](#)). It is possible that this contamination can be mitigated by removing these galaxies from the source sample, through improved photo-z methods, or with modelling approaches (e.g. [Crittenden et al. 2001](#); [Hirata et al. 2004](#); [Bridle & King 2007](#); [Hui & Zhang 2008](#); [Blazek et al. 2015](#), 2017).

ACKNOWLEDGEMENTS

Thanks to Gary Bernstein, Joe DeRose, Chris Hirata, Shivam Pandey, Judit Prat, Carles Sanchez and David Weinberg for useful discussions. JB is supported by a Swiss National Science Foundation Ambizione Fellowship. BJ is supported in part by the US Department of Energy grant desc0007901. This work used resources at the Ohio Supercomputing Center ([Ohio Supercomputer Center 1987](#)).

REFERENCES

- Baldauf T., Smith R. E., Seljak U., Mandelbaum R., 2010, *Phys. Rev. D*, **81**, 063531
- Baldauf T., Mirbabayi M., Simonović M., Zaldarriaga M., 2016, arXiv e-prints,
- Baltz E. A., Marshall P., Oguri M., 2009, *Journal of Cosmology and Astro-Particle Physics*, 2009, 015
- Berlind A. A., Weinberg D. H., 2002, *ApJ*, **575**, 587
- Bernstein G., Jain B., 2004, *ApJ*, **600**, 17
- Blazek J., McQuinn M., Seljak U., 2011, *Journal of Cosmology and Astro-Particle Physics*, 2011, 010
- Blazek J., Mandelbaum R., Seljak U., Nakajima R., 2012, *Journal of Cosmology and Astro-Particle Physics*, 2012, 041
- Blazek J., Vlah Z., Seljak U., 2015, *J. Cosmology Astropart. Phys.*, **8**, 015
- Blazek J., MacCrann N., Troxel M. A., Fang X., 2017, arXiv e-prints, p. [arXiv:1708.09247](#)
- Brainerd T. G., Blandford R. D., Smail I., 1996, *ApJ*, **466**, 623
- Bridle S., King L., 2007, *New Journal of Physics*, **9**, 444
- Bridle S. L., Crittenden R., Melchiorri A., Hobson M. P., Kneissl R., Lasenby A. N., 2002, *MNRAS*, **335**, 1193
- Bridle S., et al., 2009, *Annals of Applied Statistics*, **3**, 6
- Cacciato M., van den Bosch F. C., More S., Mo H., Yang X., 2013, *MNRAS*, **430**, 767
- Choi A., Tyson J. A., Morrison C. B., Jee M. J., Schmidt S. J., Margoniner V. E., Wittman D. M., 2012, *ApJ*, **759**, 101
- Clampitt J., et al., 2017, *MNRAS*, **465**, 4204
- Conroy C., Wechsler R. H., Kravtsov A. V., 2006, *ApJ*, **647**, 201
- Crittenden R. G., Natarajan P., Pen U.-L., Theuns T., 2001, *ApJ*, **559**, 552
- Crocce M., Castander F. J., Gaztañaga E., Fosalba P., Carretero J., 2015, *MNRAS*, **453**, 1513
- DES Collaboration et al., 2017, to be submitted to *Phys. Rev. D*
- DeRose J., et al., 2019, arXiv e-prints, p. [arXiv:1901.02401](#)
- Desjacques V., Jeong D., Schmidt F., 2018, *Phys. Rep.*, **733**, 1
- Duffy A. R., Schaye J., Kay S. T., Dalla Vecchia C., 2008, *MNRAS*, **390**, L64
- Fry J. N., Gaztanaga E., 1993, *ApJ*, **413**, 447
- Hearin A. P., Watson D. F., Becker M. R., Reyes R., Berlind A. A., Zentner A. R., 2014, *MNRAS*, **444**, 729
- Heymans C., et al., 2012, *MNRAS*, **427**, 146
- Hildebrandt H., et al., 2017, *MNRAS*, **465**, 1454
- Hirata C. M., et al., 2004, *MNRAS*, **353**, 529
- Hirata C. M., Mandelbaum R., Ishak M., Seljak U., Nichol R., Pimbblet K. A., Ross N. P., Wake D., 2007, *MNRAS*, **381**, 1197
- Hoyle B., et al., 2018, *MNRAS*, **478**, 592
- Hu W., Jain B., 2004, *Phys. Rev. D*, **70**, 043009
- Hui L., Zhang J., 2008, *ApJ*, **688**, 742
- Jain B., Taylor A., 2003, *Phys. Rev. Lett.*, **91**, 141302
- Joachimi B., Mandelbaum R., Abdalla F. B., Bridle S. L., 2011, *A&A*, **527**, A26
- Joachimi B., et al., 2015, preprint, ([arXiv:1504.05456](#))
- Joudaki S., et al., 2018, *MNRAS*, **474**, 4894
- Kaiser N., 1984, *ApJ*, **284**, L9

- Kitching T. D., et al., 2012, *MNRAS*, **423**, 3163
- Krause E., et al., 2017, arXiv e-prints, p. arXiv:1706.09359
- Leauthaud A., et al., 2012, *ApJ*, **744**, 159
- Mandelbaum R., 2018, *Annual Review of Astronomy and Astrophysics*, **56**, 393
- Mandelbaum R., Hirata C. M., Ishak M., Seljak U., Brinkmann J., 2006, *MNRAS*, **367**, 611
- Mandelbaum R., Slosar A., Baldauf T., Seljak U., Hirata C. M., Nakajima R., Reyes R., Smith R. E., 2013, *MNRAS*, **432**, 1544
- Mandelbaum R., et al., 2014, *ApJS*, **212**, 5
- Mandelbaum R., et al., 2018, *PASJ*, **70**, S25
- Miyatake H., Madhavacheril M. S., Sehgal N., Slosar A., Spergel D. N., Sherwin B., van Engelen A., 2017, *Phys. Rev. Lett.*, **118**, 161301
- Nishimichi T., et al., 2018, arXiv e-prints, p. arXiv:1811.09504
- Ohio Supercomputer Center 1987, Ohio Supercomputer Center, <http://osc.edu/ark:/19495/f5s1ph73>
- Peacock J. A., Smith R. E., 2000, *MNRAS*, **318**, 1144
- Prat J., et al., 2018a, arXiv e-prints, p. arXiv:1810.02212
- Prat J., et al., 2018b, *Phys. Rev. D*, **98**, 042005
- Schaye J., et al., 2010, *MNRAS*, **402**, 1536
- Schaye J., et al., 2015, *MNRAS*, **446**, 521
- Seljak U., 2000, *MNRAS*, **318**, 203
- Singh S., Mandelbaum R., 2016, *MNRAS*, **457**, 2301
- Singh S., Mandelbaum R., Seljak U., Rodríguez-Torres S., Slosar A., 2018, arXiv e-prints, p. arXiv:1811.06499
- Smith R. E., et al., 2003, *MNRAS*, **341**, 1311
- Smith R. E., Scoccimarro R., Sheth R. K., 2007, *Phys. Rev. D*, **75**, 063512
- Springel V., et al., 2018, *MNRAS*, **475**, 676
- Takahashi R., Sato M., Nishimichi T., Taruya A., Oguri M., 2012, *ApJ*, **761**, 152
- Tanaka M., et al., 2018, *PASJ*, **70**, S9
- Tasitsiomi A., Kravtsov A. V., Wechsler R. H., Primack J. R., 2004, *ApJ*, **614**, 533
- Taylor A. N., Kitching T. D., Bacon D. J., Heavens A. F., 2007, *MNRAS*, **374**, 1377
- Tinker J. L., Robertson B. E., Kravtsov A. V., Klypin A., Warren M. S., Yepes G., Gottlöber S., 2010, *ApJ*, **724**, 878
- Troxel M. A., Ishak M., 2014, *Phys. Rev. D*, **89**, 063528
- Tyson J. A., Valdes F., Jarvis J. F., Mills Jr. A. P., 1984, *ApJ*, **281**, L59
- Velander M., et al., 2014, *MNRAS*, **437**, 2111
- Viola M., et al., 2015, *MNRAS*, **452**, 3529
- Vogelsberger M., et al., 2014, *MNRAS*, **444**, 1518
- Wechsler R. H., Tinker J. L., 2018, *Annual Review of Astronomy and Astrophysics*, **56**, 435
- Weinberg D. H., Mortonson M. J., Eisenstein D. J., Hirata C., Riess A. G., Rozo E., 2013, *Phys. Rep.*, **530**, 87
- Wibking B. D., et al., 2019, *MNRAS*, **484**, 989
- Zuntz J., et al., 2015, *Astronomy and Computing*, **12**, 45
- van Uitert E., et al., 2016, *MNRAS*, **459**, 3251
- van Uitert E., et al., 2018, *MNRAS*, **476**, 4662

This paper has been typeset from a $\text{\TeX}/\text{\LaTeX}$ file prepared by the author.